frontiers in Sensors

ORIGINAL RESEARCH
published: 21 March 2022
doi: 10.3389/fsens.2022.865215

Periodic Collapsed Solid-Core PCF Based Modal Interferometer for Chemical Sensing

Jitendra Narayan Dash[1,2] *and Rajan Jha*[2]*

[1]Photonics Research Center, Department of Electrical Engineering, The Hong Kong Polytechnic University, Kowloon, Hong Kong SAR, China, [2]Nanophotonics and Plasmonics Laboratory, School of Basic Sciences, Indian Institute of Technology Bhubaneswar, Bhubaneswar, India

We experimentally demonstrated a periodically collapsed solid-core photonic crystal fiber (SCPCF) based modal interferometer for sensing refractive index (RI) of chemicals. A given piece of SCPCF is periodically collapsed using an easily and widely available commercial splicer machine and a micropositioner. The distance between the collapsed and number of collapsed regions can be controlled precisely by the inexpensive micropositioner. The effect of the number of periods on the RI sensitivity has been studied. Our experimental results show that this simple and easily fabricated interferometer has an RI sensitivity of 230 nm/RIU with negligible cross-temperature error.

OPEN ACCESS

Edited by:
Joel Villatoro, School of Engineering, University of the Basque Country, Spain

Reviewed by:
Daniel Jauregui-Vazquez, University of Guanajuato, Mexico
Ginu Rajan, University of Wollongong, Australia

***Correspondence:**
Rajan Jha
rjha@iitbbs.ac.in

Specialty section:
This article was submitted to Physical Sensors, a section of the journal Frontiers in Sensors

Received: *29 January 2022*
Accepted: *25 February 2022*
Published: *21 March 2022*

Citation:
Dash JN and Jha R (2022) Periodic Collapsed Solid-Core PCF Based Modal Interferometer for Chemical Sensing. Front. Sens. 3:865215. doi: 10.3389/fsens.2022.865215

Keywords: photonic crystal fiber (PCF), modal interference, chemical sensing, optical fiber device, interferometry techniques

1 INTRODUCTION

Fiber-based interferometers have been widely used in the field of sensing due to their high accuracy, stability, electromagnetic immunity, and remote sensing capability. Different interferometry-based configurations such as Mach-Zehnder, Michelson, and Sagnac loop have been proposed for various sensing applications using conventional fibers (Cao et al., 2015; Liang et al., 2015; Luo et al., 2015; Shao et al., 2015). SCPCFs can be used as an alternative to conventional fiber-based interferometers due to their several attractive features such as endlessly single-mode property, large mode area, and tunability of geometrical parameters (Jha et al., 2009; Dash et al., 2015; Dash and Jha, 2015; Zhao et al., 2015). Further, the stronger evanescent field in SCPCF makes it preferable for sensors based on interferometry (Wang et al., 2013). SCPCFs have been used in different interferometric setups such as SMF-SCPCF splicing and tapered PCF for sensing applications (Jha et al., 2009; Zhao et al., 2015). Periodic variation of refractive index along the length of PCF has also been utilized for various sensing applications (Bock et al., 2007; Lázaro et al., 2010; Wang et al., 2013; Iadicicco et al., 2015; Zhong et al., 2015). For example, periodically tapered long-period grating (LPG) written in SCPCF and periodically tapered SCPCF have been utilized for pressure and refractive index sensing, respectively (Bock et al., 2007; Wang et al., 2013). However, the LPG-based pressure sensor has not explained the effect of change of the refractive index of the surrounding environment around the periodically collapsed region. Although the periodically tapered SCPCF has been utilized for RI sensing, a high-power, expensive CO_2 laser is required to develop this system (Wang et al., 2013). Moreover, in this case, the interference pattern is formed due to the effect of periodic variation of the refractive index because of the partial or complete collapse of the air holes (Wang et al., 2013). However, there is no interference pattern formation due to the splicing of SMF and SCPCF. Therefore, the effect of periodic variation of the collapsed region on the interference pattern formed due to the splicing of SMF and PCF has not been studied and analyzed. In addition to the

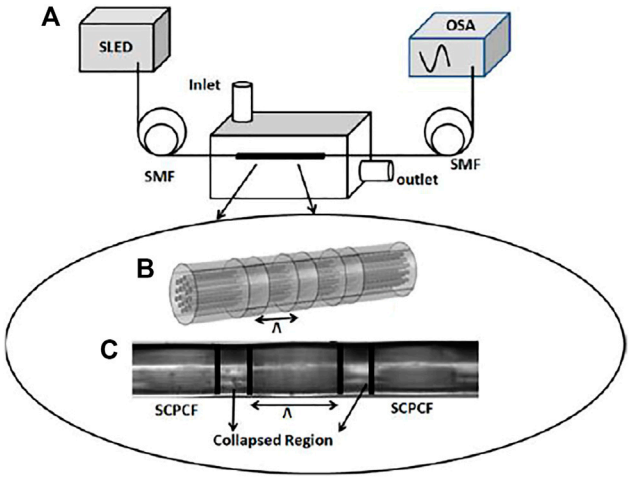

FIGURE 1 | (A) Schematic of the proposed experimental setup. **(B,C)** Schematic of the SCPCF with collapsed region and the microscopic image of the collapsed region, respectively.

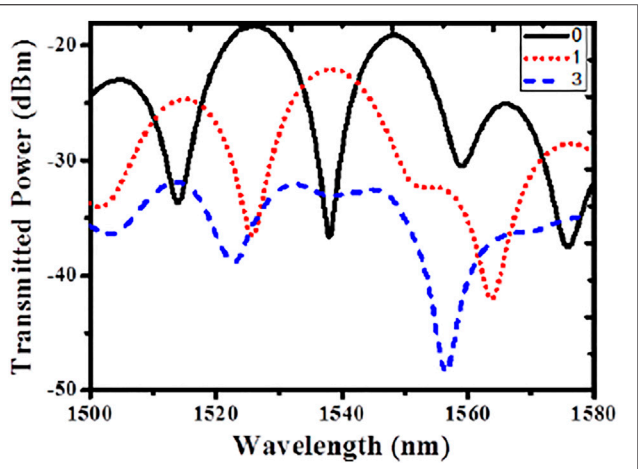

FIGURE 2 | Variation in the interference pattern with increase in number of collapsed regions.

abovementioned sensors, LPGs have also been written on SCPCF and hollow-core PCF (HCPCF), respectively (Iadicicco et al., 2015; Zhong et al., 2015). However, LPG has been written on SCPCF by periodic inflation of holes using a femtosecond laser, which is neither economical nor easy to operate and involves complex and expensive systems (Zhong et al., 2015). Moreover, in the case of HCPCF-based LPG, RI sensing has not been analyzed, and fabrication requires more careful observation of the collapse of holes as the percentage of air content is more than SCPCF(Iadicicco et al., 2015).

This study analyzes the effect of air holes' periodic collapse on the performance of SCPCF-based modal interferometer used for chemical sensing applications. The periodic collapse of air holes has been achieved using a commercial splicing machine and a micropositioner, which are simple and economical. Furthermore, this method does not require any complex optical arrangements. The arc current of the splicer has also been optimized to realize a complete collapse of air holes arranged periodically along the length of SCPCF.

2 FABRICATION OF PROBE

A short section of SCPCF (LMA 8, NKT Photonics) is spliced between two conventional SMFs, with one of the SMF connected to a broadband source, whereas the other end is connected to an optical spectrum analyzer (OSA). The core and cladding diameters of PCF were 8.5 and 125 μm, respectively. Seven rings of air holes arranged in triangular geometry surround the core. The air holes' average diameter (d) is 2.32 μm, with a pitch (Λ) of 5.6 μm. The mode field diameter was 7 ± 1 μm, whereas the filling factor d/Λ was 0.414. The splicing of SMF with SCPCF leads to the collapse of air holes over an approximate distance of 220 μm on both sides of SCPCF. The arc power and arc time for splicing of SMF with PCF were Std-20 and 2000 milliseconds, respectively, where the term Std refers to the standard value. The SMF spliced SCPCF is placed in the splicer machine so that the middle portion of SCPCF remains between the two electrodes of the splicer, and the spliced SMFs are fixed in V-grooves of two micropositioners (Nanomax, Thorlabs), with a pitch of 10 μm. One of the SMFs is completely fixed on the micropositioner while the other SMF remains free so that it can move. When an arc is applied, the holes of the SCPCF completely collapse over an approximate distance of 120 μm. The arc current and arc time are optimized such that the holes of the SCPCF collapse with negligible taper. After each arc, the SMF is moved to one side by a fixed distance (Λ) with the help of a micropositioner, thereby resulting in SCPCF displacement by the same distance. Repeating this procedure, we fabricated the desired probe with a particular period Λ and the number of periods' n (number of collapsed regions). In addition to this, n can easily be varied using this simple, which is an easily available and cost-effective technique. In principle, the value of Λ can be tailored by proper choice of the pitch of the micropositioner. We also fabricated three samples of SCPCF with the number of periods n = 5, 9, and 14 for a constant period Λ = 300 μm. These probes with different numbers of periods have been characterized and used to analyze the response of the sensor for chemical sensing along with temperature study.

3 EXPERIMENTAL SETUP AND RESULTS

The schematic of the experimental setup is shown in **Figure 1A**. Light is launched into the fabricated probe from a broadband source (Super Luminescent Light Emitting Diode), and the transmitted light is analyzed using OSA. The sensing region—the periodic collapsed SCPCF—is kept in a container of the analyte. The schematic of the periodic collapsed SCPCF is shown in **Figure 1B**, whereas the microscope image of the same is shown in **Figure 1C**. As shown in **Figure 1C**, the holes are completely collapsed along the length of SCPCF. Accordingly, the

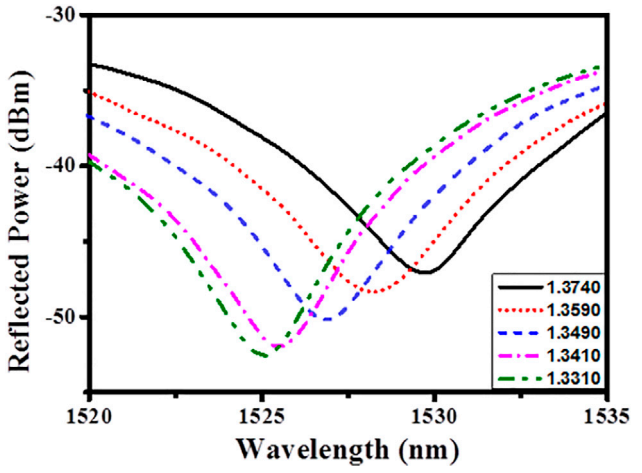

FIGURE 3 | Shift in interference pattern with RI of different chemicals and n is fixed at 5.

refractive index of SCPCF's collapsed region differs from that with air holes, resulting in a periodic variation of refractive index along the length of SCPCF. During the formation of the collapsed region, we continuously monitored the interference pattern of the transmission spectrum for different n values, as shown in **Figure 2**. The variation in the transmitted power with wavelength significantly changes with an increase in the number of collapsed regions. Following the above procedure, we have fabricated three probes, with the number of periods n being 5, 9, and 14.

When light is coupled from SLED to the probe, the fundamental mode of the SMF diffracts and broadens at the collapsed region at the junction of SMF and SCPCF, resulting in the excitation of core and cladding modes in SCPCF. The modes with different propagation constant propagate along the length of SCPCF acquiring different phases depending upon the length of SCPCF. The phase difference leads to the formation of the interference pattern when these modes interfere at the first collapsed region. The intensity of the intensity pattern after the first collapsed region is given by

$$I = I_{co} + I_{cl} + 2\sqrt{I_{co}I_{cl}}\cos\left(\Delta n_{eff} L_p / \lambda\right) \quad (1)$$

where L_p is the length of the SCPCF and Δn_{eff} is the difference between the effective index of core and cladding mode in the uncollapsed SCPCF. When the collapsed region along with SCPCF is dipped in analyte, the change in the effective index of cladding mode in the uncollapsed SCPCF and the periodically collapsed SCPCF change, resulting in a shift of the interference pattern.

We have used different chemicals such as isopropanol, ethanol, hydrogen peroxide, and methanol sucrose solutions with different refractive indices to investigate the refractive index sensitivity of the proposed sensor. The refractive indices of the chemicals are first calibrated using an Abbe refractometer. The collapsed section of SCPCF, along with the splicing region of

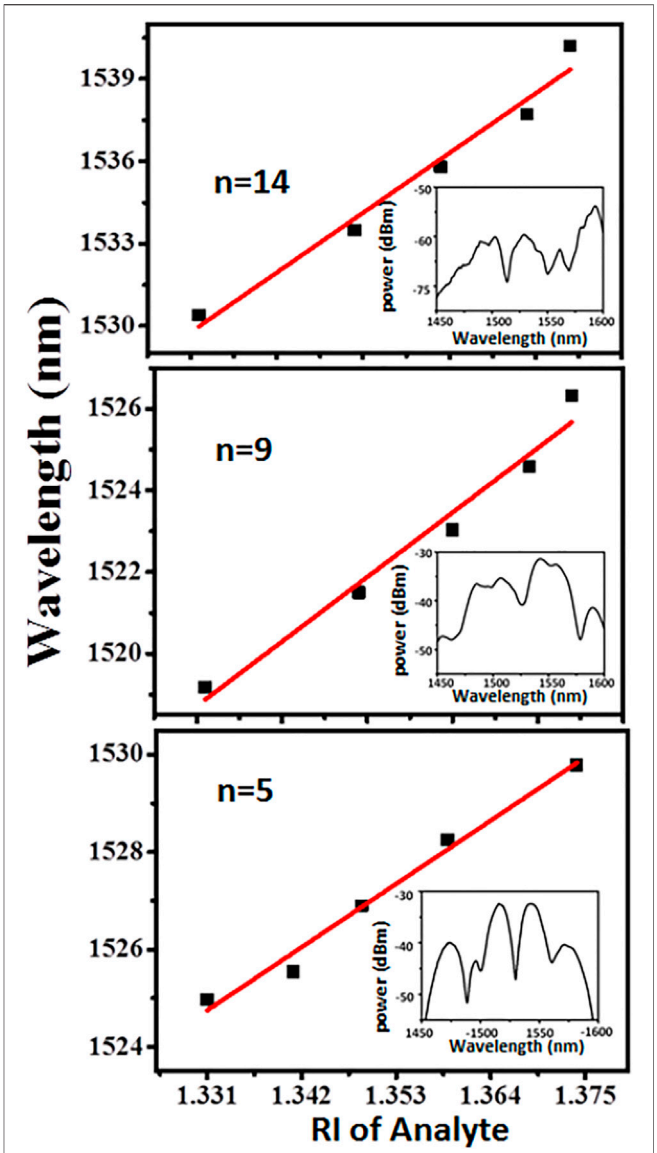

FIGURE 4 | Shift in interference pattern with RI of chemicals. The black squares show the experimental data, and the red lines show the linear fit.

SMF and SCPCF, was kept in a small container containing the analyte, with an inlet and outlet, as shown in **Figure 2**. After each measurement, the probe is dried with dry nitrogen to ensure that the interference pattern returns to its original position. First, we kept one of the three probes with n = 5 and Λ= 300 μm in the container. When the refractive index of the analyte is changed from 1.3310 to 1.3740, the dip of the interference pattern shifts from 1,524.97 nm to 1,529.79 nm, as shown in **Figure 3**. Similarly, the response of the probe for probes with the number of periods of 9 and 14 is investigated. We found that the dip of the interference pattern shifts from 1,519.18 nm to 1,526.32 nm and from 1,530.4 nm to 1,540.2 nm for the probes with the number of periods of 9 and 14, respectively. The shift of the wavelength of the dip of the interference pattern with change in RI of analyte is shown in **Figure 4**. The shift is linear, which is

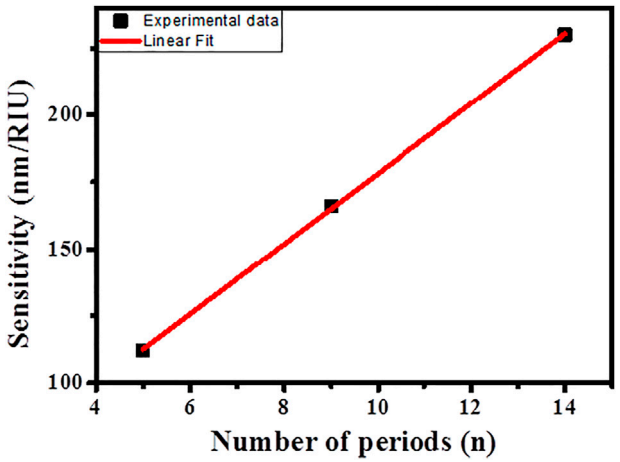

FIGURE 5 | Variation in sensitivity with number of collapsed regions.

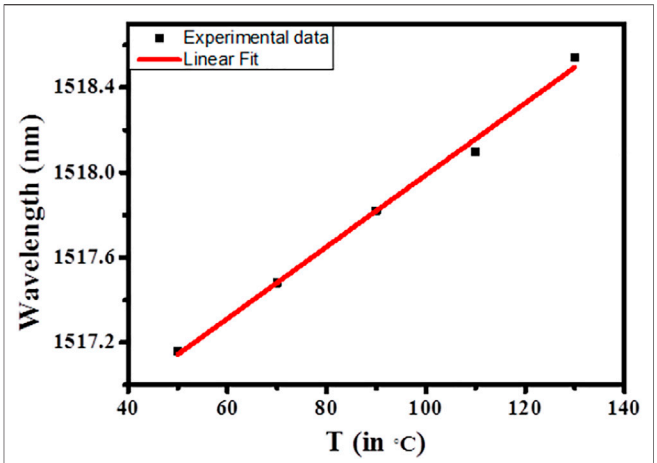

FIGURE 7 | Shift in wavelength of dip with temperature.

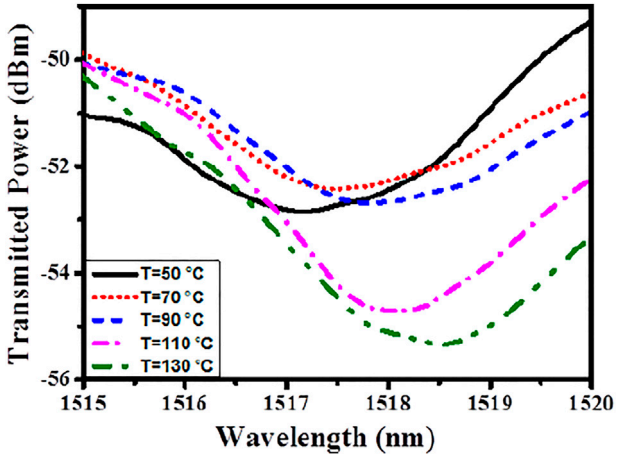

FIGURE 6 | Shift in interference pattern with temperature.

the best choice for sensing applications. The power loss in our case increases with the increase in the number of collapsed regions. The loss is more compared to LPG-based sensors (Bock et al., 2007; Zhong et al., 2015) because of the presence of a completely collapsed region and the reflection of light from each of the air hole silica interface. As shown in **Figure 4**, the loss is maximum (−74 dBm) for configuration with 14 perturbations.

The wavelength sensitivity, defined as the ratio of the shift in wavelength of dip to the change in RI of the analyte, is calculated for all three samples. The probe with $n = 14$ showed a wavelength sensitivity of 230 nm/RIU, whereas the probes with the number of periods 5 and 9 showed a sensitivity of 112 nm/RIU and 166 nm/RIU, respectively. The sensitivity variation for the three probes with different numbers of periods is shown in **Figure 5**. Sensitivity increases linearly with an increase in the number of periods. The sensitivity of 230 nm/RIU is higher than what was previously reported (Wang and Tang, 2012; Wang et al., 2014; Ni et al., 2016; Dash et al., 2020). Considering the resolution of OSA as 0.01 nm, the resolution of the proposed sensor was 4.34×10^{-5} RIU. This is comparable to commercially available spectrometers. In principle, the distance between the collapsed regions (Λ) can easily be tuned by proper choice (pitch) of micropositioner to optimize the sensor's performance using this easy fabrication technique. Apart from external analyte and parameters such as n and Λ, the number of collapsed regions, the interference pattern also gets affected by temperature change. However, as the spliced and collapsed regions are permanent, the nature of the interference pattern is not affected by a small change in temperature. Therefore, temperature compensation may not be needed in these refractometers.

In order to investigate the effect of temperature on the interference pattern, we kept the periodic collapsed SCPCF along with the SMF on a hot plate. When the hot plate temperature is gradually increased from 50°C to 130°C, the interference pattern shifts from 1,517.16 to 1,518.54 nm, as shown in **Figure 6**.

The shifting of interference pattern toward higher wavelength occurs due to the positive thermal expansion and thermo-optic coefficient of silica. The variation of the wavelength of the dip with temperature can be explained by (Wang and Wang, 2012)

$$\Delta\lambda_{\min} = \frac{2}{m}\left(n_s \times \frac{d(L_P)}{dT} \times \Delta T + \left(L_p\right) \times \frac{dn_s}{dT} \times \Delta T\right)$$

where L_p is the length of SCPCF, n_s is the RI of silica, and m is the order of the interference dip. With an increase in temperature, L_p and n_s increase due to the positive thermal expansion and thermo-optic coefficient of silica. The thermos-optic coefficient of air in the holes of SCPCF is neglected as its value is nearly zero. The shifting of the wavelength of dip of interference pattern with temperature is linear, as shown in **Figure 7**. Moreover, the temperature sensitivity of the proposed structure is calculated as 13.8 pm/°C. Although this sensitivity is more than (Bock et al., 2007), it is significantly less than the shift due to the change in RI of the analyte. The cross-sensitivity is 6×10^{-5} RIU/°C by considering the RI and temperature sensitivity of the sensor.

The low cross-temperature sensitivity can be attributed to the absence of dopants in the core and the presence of air holes in PCF. As the effect of temperature is almost insignificant compared to that due to the refractive index of the analyte, the proposed structure can be used as a temperature-insensitive sensor.

4 CONCLUSION

An SCPCF-based modal interferometric sensor incorporating periodic collapsed air holes has been reported. The periodic collapsed SCPCF has been fabricated with the help of a micropositioner and a commercial splicer machine. The number of periods has been varied using this simple and economical technique. The proposed interferometer shows a RI sensitivity of 230 nm/RIU along with a resolution of 4.34×10^{-5} RIU. Moreover, the sensor is temperature-insensitive, with a temperature sensitivity of 13.8 pm/°C. Due to low-temperature sensitivity, temperature compensation may not be required in these refractometers. The low-cost proposed sensor can sense different physical parameters such as strain and pressure.

DATA AVAILABILITY STATEMENT

The raw data supporting the conclusion of this article will be made available by the authors without undue reservation.

AUTHOR CONTRIBUTIONS

JND and RJ contributed to conceptualization. JND did the experiment. Both contributed to manuscript preparation.

ACKNOWLEDGMENTS

RJ acknowledges BRNS, SERB STAR Fellowship.

REFERENCES

Bock, W. J., Chen, J., Mikulic, P., Eftimov, T., and Korwin-Pawlowski, M. (2007). Pressure Sensing Using Periodically Tapered Long-Period Gratings Written in Photonic crystal Fibres. *Meas. Sci. Technol.* 18, 3098–3102. doi:10.1088/0957-0233/18/10/s08

Cao, Y., Liu, H., Tong, Z., Yuan, S., and Su, J. (2015). Simultaneous Measurement of Temperature and Refractive index Based on a Mach-Zehnder Interferometer Cascaded with a Fiber Bragg Grating. *Opt. Commun.* 342, 180–183. doi:10.1016/j.optcom.2014.12.067

Dash, J. N., Jha, R., Villatoro, J., and Dass, S. (2015). Nano-displacement Sensor Based on Photonic crystal Fiber Modal Interferometer. *Opt. Lett.* 40, 467–470. doi:10.1364/OL.40.000467

Dash, J. N., Jha, R., and Das, R. (2020). Micro-air Cavity Incorporated Tapered-Tip Photonic crystal Fiber Based Compact Refractometer. *Laser Phys. Lett.* 17, 055101. doi:10.1088/1612-202x/ab8738

Dash, J. N., and Jha, R. (2015). Inline Microcavity Based PCF Interferometer for Refractive index and Temperature Sensing. *IEEE Photon. Technol. Lett.* 27, 12. doi:10.1109/lpt.2015.2421308

Iadicicco, A., Ranjan, R., and Campopiano, S. (2015). Fabrication and Characterization of Long-Period Gratings in Hollow Core Fibers by Electric Arc Discharge. *IEEE Sensors J.* 15 (5), 3014–3020. doi:10.1109/jsen.2014.2383175

Jha, R., Villatoro, J., Badenes, G., and Pruneri, V. (2009). Refractometry Based on a Photonic crystal Fiber Interferometer. *Opt. Lett.* 34, 617–619. doi:10.1364/ol.34.000617

Lázaro, J. M., Quintela, A., Urbanczyk, W., Wojcik, J., and Lopez-Higuera, J. M. (2010). Bragg Gratings Written in Tapered Solid-Core Photonic Crystal Fibers" IEEE Photon. *Tech. Lett.* 22 (14), 1048–1050.

Liang, X., Liu, Z., Wei, H., Li, Y., and Jian, S. (2015). Detection of Liquid Level with an Mi-Based Fiber Laser Sensor Using Few-Mode EMCF. *IEEE Photon. Technol. Lett.* 7, 8. doi:10.1109/lpt.2015.2389857

Luo, H., Sun, Q., Xu, Z., Jia, W., Liu, D., and Zhang, L. (2015). Microfiber-based Inline Mach–Zehnder Interferometer for Dual-Parameter Measurement. *IEEE Photon. J.* 7, 2. doi:10.1109/jphot.2015.2395133

Ni, X., Wang, M., Guo, D., Hao, H., and Zhu, J. (2016). A Hybrid Mach-Zehnder Interferometer for Refractive Index and Temperature Measurement. *IEEE Photon. Technol. Lett.* 28 (17), 1850–1853. doi:10.1109/lpt.2016.2558209

Shao, L.-Y., Luo, Y., Zhang, Z., Zou, X., Luo, B., Pan, W., et al. (2015). Sensitivity-enhanced Temperature Sensor with Cascaded Fiber Optic Sagnac Interferometers Based on Vernier-Effect. *Opt. Commun.* 336, 73–76. doi:10.1016/j.optcom.2014.09.075

Wang, J.-N., and Tang, J.-L. (2012). Photonic crystal Fiber Mach-Zehnder Interferometer for Refractive index Sensing. *Sensors* 12, 2983–2995. doi:10.3390/s120302983

Wang, P., Bo, L., Guan, C., Semenova, Y., Wu, Q., Brambilla, G., et al. (2013). Low-temperature Sensitivity Periodically Tapered Photonic crystal-fiber-based Refractometer. *Opt. Lett.* 38 (19), 3795–3798. doi:10.1364/ol.38.003795

Wang, P., Ding, M., Bo, L., Guan, C., Semenova, Y., Sun, W., et al. (2014). Photonic crystal Fiber Half-Taper Probe Based Refractometer. *Opt. Lett.* 39 (7), 2076–2079. doi:10.1364/ol.39.002076

Wang, T., and Wang, M. (2012). Fabry-Pérot Fiber Sensor for Simultaneous Measurement of Refractive Index and Temperature Based on an In-Fiber Ellipsoidal Cavity. *IEEE Photon. Technol. Lett.* 24 (19), 1733–1736. doi:10.1109/lpt.2012.2212184

Zhao, Y., Wu, D., and Lv, R. (2015). Magnetic Field Sensor Based on Photonic Crystal Fiber Taper Coated with Ferrofluid. *IEEE Photon. Technol. Lett.* 27, 1. doi:10.1109/lpt.2014.2360531

Zhong, X., Wang, Y., Liao, C., Liu, S., Tang, J., and Wang, Q. (2015). Temperature-insensitivity Gas Pressure Sensor Based on Inflated Long Period Fiber Grating Inscribed in Photonic crystal Fiber. *Opt. Lett.* 40 (8), 1791–1794. doi:10.1364/ol.40.001791

Conflict of Interest: The authors declare that the research was conducted in the absence of any commercial or financial relationships that could be construed as a potential conflict of interest.

Publisher's Note: All claims expressed in this article are solely those of the authors and do not necessarily represent those of their affiliated organizations or those of the publisher, the editors, and the reviewers. Any product that may be evaluated in this article, or claim that may be made by its manufacturer, is not guaranteed or endorsed by the publisher.